Corrosion Performance of Steel Rebars by Application of Electroless Ni-P-W Coating - An Optimization Approach using Grey Relational Analysis

Arkadeb Mukhopadhyay
Assistant Professor
Department of Mechanical Engineering
Birla Institute of Technology Mesra, Ranchi
India

Sarmila Sahoo
Associate Professor
Department of Civil Engineering
Heritage Institute of Technology, Kolkata
India

Electroless deposited Ni-P-W coatings were investigated as a potential candidate for corrosion prevention of steel rebars subjected to chloride environment. Potentiodynamic polarization was utilized to test corrosion resistance of bare and coated rebars. Taguchi based grey relational analysis was used to predict a bath composition that would result in enhanced corrosion resistance of the coated rebars. Higher corrosion potential (-258 mV) and low corrosion current density (0.065 $\mu A/cm^2$) could be achieved compared to bare rebars (-653 mV, 11.7 $\mu A/cm^2$) for a nickel sulphate concentration of 30 g/l, sodium hypophosphite concentration of 17 g/l and sodium tungstate concentration of 20 g/l in the coating bath. The morphology of the bare and coated rebars post corrosion revealed severe cracking of the bare rebars. While the Ni-P-W coated rebar at optimal bath combination predicted by Taguchi method suffered negligible damage in chloride environment with the onset of an oxide layer.

Keywords: *Concrete, Steel rebars, Potentiodynamic Polarization, Ni-P-W coating, Optimization.*

1. INTRODUCTION

Concrete reinforced with steelrebars are versatile materials widely used for construction of structures. Because of the porosity in concrete, it is very likely that the rebars and the lifetime of structures are affected by corrosion. Premature failure of concrete takes place due to chloride induced attacks [1, 2]. A considerable financial loss may take place and lead to high cost of repair. Steel rebar corrosion in concrete is a rather complex phenomenon and affected by its working environment and guided by complex electrochemical reactions [3, 4]. Chloride ion penetration and nation causes severe degradation of concrete structures in marine environment [5, 6]. In fact, chloride attack also plays an important role in corrosion of reinforced rebars exposed to sewer along with biogenic sulfuric acid and hydrogen disulfide [7].

In ordinary Portland cement, a thin passivating layer of oxide is formed on the rebar in alkaline environment (pH>13) which makes it corrosion resistant [8]. But as the chloride concentration increases beyond a certain threshold value, this passivity is lost [9-11]. Furthermore, interaction with atmospheric CO_2 also decreases the pH [3]. In marine environment, coastal structures, bridges, etc., due to a high accumulation of chloride ions, severe degradation of steel rebars embedded in concrete takes place [12]. The localized attack of chlorides causes rapid reduction in cross-section and failure of the structure [3]. Also, environment mediated embrittlement of microstructure of rebars may take place along with pitting causing structural steels to crack under stress [13]. The applied loading condition may also aggravate the corrosion of stainless steel rebars when exposed to pitting attack of chlorides [14].

To counteract the detrimental effects of chloride attack on the lifetime of structures, it is necessary to take protective measures and research is still ongoing. The strategies for improvement of the corrosion resistance include modifying the concrete composition, suitable selection of reinforcement steel and application of protective coatings to the steel rebars. Admixtures in the concrete tend to inhibit corrosive action of chlorides and induce self-healing characteristics [15, 16]. Such admixtures may include minerals, nitrite ions, organic inhibitors, inorganic inhibitors, aminoalcohol, phosphate-based inhibitor, etc. [17-24]. Sodium molybdate also acts as an efficient inhibitor for prevention of rebar corrosion in concrete exposed to adverse conditions and coastal areas [25].

Selecting suitable grade of steel prevents corrosion of rebars. Electrochemical study revealed that stainless steel of austenitic grade remained passive in simulated seawater which led to enhanced corrosion resistance compared to carbon steel rebars [12]. High chromium steel rebars had high corrosion resistance in chloride environment compared to mild steel [26]. High ratio of Cr/Fe and presence of molybdates in passive film resulted in high corrosion resistance of stainless steels (AISI 316L) to pitting corrosion of chlorides [27]. Electrochemical studies also revealed that austenitic microstructure was more resistant to corrosion in simulated concrete pore solution with varying chloride content compared to ferritic microstructure [28]. Other

Received: December 2020, Accepted: February 2021
Correspondence to: Dr Sarmila Sahoo
Heritage Institute of Technology,
Kolkata 700107, India
E-mail: sarmila.sahoo@gmail.com
doi:10.5937/fme2102445M

research works also revealed that chromium modified steel rebars had higher corrosion resistance due to the formation of a dense and compact passive film [29, 30].

The surface of rebars may be engineered with barrier or sacrificial coatings for prevention of corrosion. Epoxy coatings provide a combination of good bond strength with concrete along with good corrosion resistance [31]. Electrochemical tests revealed that even over a two-year period, epoxy coatings showed no damage to the underlying mild steel reinforcement to severe attack of chlorides [32]. Infact self-healing capabilities could be induced in epoxy coatings (along with 10% microencapsulated tung oil) and offered remarkable corrosion resistance even in damaged condition [33]. Epoxy coatings with nano-fillers significantly improve the erosion and corrosion resistance of rebars in saline media [34, 35]. Electrochemical studies also revealed that concrete reinforcing steel used in bridges in regions where deicing salt is used can be protected efficiently from damage caused by chloride infiltration using epoxy coating [36]. On the other hand, enamel coatings are also popular for corrosion protection of steel rebars. Pure/double enamel coatings offer high resistance to corrosion attacks compared to mixed enamel coatings or bare rebars in 3.5% NaCl or at various chloride concentrations [37-39]. Over a period of 244 days, pure enamel coatings were seen to outperform both double enamel or mixed enamel coatings [40]. Fusion bonded epoxy coatings had even lower corrosion rates [40]. But enamel coatings suffer from the disadvantage of getting damaged during transportation and hence require careful handling. In such a case, duplex coating with inner enamel and outer epoxy layers provide necessary protection from delamination and 180% improved corrosion resistance compared to the individual coatings [41]. The lifetime of concrete exposed to chloride attacks can be also extended by hot-dip galvanizing of the reinforcement steel [42]. Galvanized steel embedded in ultra-high-performance concrete in 3.5% NaCl was monitored over a period of 1 year [43]. Open circuit potential (OCP) and tafel polarization revealed that the rebars were in passive state. Remarkable corrosion performance in severe chloride contamination was also seen over a period of 2 years [44]. Nevertheless, porosity of concrete increased due to the formation of hydrogen during reaction of zinc coating with fresh cement during the initial stages [45].

High corrosion resistance was offered by electroless Ni-P coatings that prove to be potential candidates for providing barrier protection to rebars. Steel rebars with Ni-P coatings subjected to simulated concrete pore solution offered a high degree of corrosion resistance even with chloride contamination [46]. The protective ability of binary Ni-P and poly-alloy coatings in 3.5% NaCl (approximately simulated marine environment) was revealed in a recent study [47]. The coating variants could effectively shield Fe-600 grade steel rebars from pitting chloride attacks. Initially, from electrochemical tests it was concluded that Ni-P-W coating had the highest protective ability i.e. nobler corrosion potential and low corrosion current density [47]. The present work thus aims to improve the corrosion resistance of electroless Ni-P-W coated steel rebar to a further extent in 3.5% NaCl solution since such areas have been scantily addressed. It is well known that the properties of electroless nickel coatings can be tailored by controlling the bath composition [48]. Thus, an effective bath formulation may further enhance the protective ability of the coating in harsh marine environments and chloride attacks.

In the present work, Fe-600 grade rebars were coated with Ni-P-W coatings by electroless method. The bath composition i.e. source of nickel, phosphorus and tungsten was varied following Taguchi's experimental design to minimize the number of trial runs. Corrosion resistance of bare and coated rebars was measured using electrochemical techniques. The corrosive media considered was 3.5% NaCl. This has been done for the simulation of harsh chloride attack that is experienced by concrete in coastal environments. The corrosion current density and potential obtained from tafel polarization was optimized simultaneously using grey relational analysis. Apart from coating bath optimization, characterization of the deposited coatings was carried out using scanning electron microscope, energy dispersive X-ray spectroscopy and X-ray diffraction techniques. Corrosion mechanism of the bare and coated rebars was also investigated to gain a deeper insight into the corrosion behavior in chloride environment.

2. EXPERIMENTAL DETAILS

Ni-P-W coatings were deposited on Fe-600 grade steel rebars (IS 1786:2008) and are in variance with provisions laid down in ISO 6935-2:2007 based on geographical and technological factors along with construction practices adopted in India [49]. Composition of the rebar was 0.3% C, 0.040% P and 0.040% S while the rest being Fe. The specimens were carefully prepared before coating deposition and the steps are shown in Fig. 1.

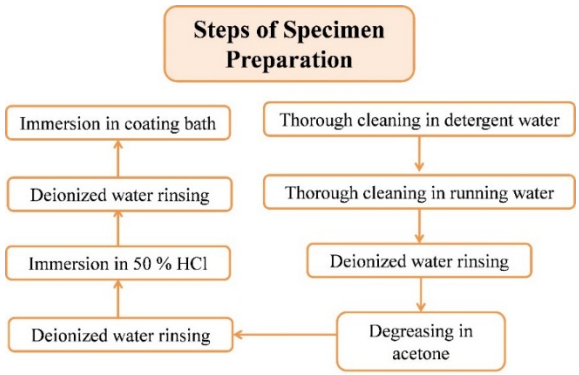

Figure 1. Steps of specimen preparation

The rebars were ground to N5 roughness grade (0.4 μm Ra). Bath parameters and deposition conditions are shown in Fig. 2. The coating bath composition was based on a previous research work [47] which yields average coating thickness of 25μm. The Ni, P and W content were varied by varying concentration of nickel sulphate, sodium hypophosphite and sodium tungstate in the coating bath in three uniformly spaced levels. They were also the process parameters of the experimental optimization and listed in Table 1. The process parameters and their levels were selected based on previous work and careful study of literature [47, 48,

50, 51]. After deposition, rinsing in deionized water was carried out following which the specimens were dried. Any heat treatment or thermochemical treatment was not applied to the coated specimens. Several Fe-600 steel specimens were coated by varying nickel sulphate, sodium hypophosphite and sodium tungstate (Table 1). A significant reduction in the number of experimental trials occurred by adopting Taguchi's orthogonal array (OA) of experiments. L9 array was chosen accordingly. The different combination of the process parameters as per L9 OA is listed in Table 2.

Table 1. Factors varied in the coating bath

Factors	Units	Code	Levels		
			1	2	3
Nickel sulphate	g/L	A	20*	25	30
Sodium hypophosphite	g/L	B	14	17	20*
Sodium tungstate	g/L	C	15	20	25*
*Initial test run combination (A1B3C3)					

Table 2. Experimental combinations given in L9 array

Exp. No.	A	B	C
1	1	1	1
2	1	2	2
3	1	3	3
4	2	1	2
5	2	2	3
6	2	3	1
7	3	1	3
8	3	2	1
9	3	3	2

A three-electrode electrochemical cell was utilized to measure the corrosion resistance (GILL AC, ACM INSTRUMENTS). Potentiodynamic polarization (PDP) tests were carried out for the Ni-P-W electroless coatings in 3.5% NaCl. The area of the exposed rebars in the three-electrode cell pre and post coating deposition was ~1 cm^2 which was also the working electrode (WE). The reference electrode (RE) was saturated calomel while the auxillary electrode (AE) was a platinum rod. Polarization of the WE in anodic and cathodic direction was carried out at 1 mV/s and within ± 250 mV vs. OCP. A settling time of 15 min was given for OCP stabilization. The corrosion current density (I_{corr}) and potential (E_{corr}) was obtained from tafel extrapolation plots.

Optimal bath parameters were obtained using grey relational analysis (GRA). GRA is a simple and cost-effective multi-criteria decision-making method to optimize system performance in minimum number of experiments when coupled with Taguchi's OA [52]. Here, the performance measures or system response parameters were E_{corr} and I_{corr}. While the process parameters or system variables were those mentioned in Table 1. This multi-variate and multi-objective optimization are converted to single response optimization by obtaining the grey relational grade (GRG). It may be noted here that the present case is a multi-objective optimization since higher corrosion resistance is denoted by lower I_{corr} and higher value (more noble) of E_{corr}. The steps of GRA are illustrated schematically in Fig. 3. Statistical analysis of the GRG was also carried out to understand the degree of influence of the bath parameters on the corrosion resistance.

Some of the deposited coatings were characterized using scanning electron microscopy (SEM), Energy dispersive X-ray spectroscopy (EDS) and X-ray diffraction (XRD) techniques. Surface morphology was observed using SEM (JEOL, JSM 6390 and SIGMA – 300, ZEISS). EDS analysis was carried out alongside SEM for composition determination (EDAX CORPORATION). XRD was carried out at 1°/min scanning rate using CuKα source and for a range of 20-80° 2θto analyze the coating structure (RIGAKU, SMARTLAB). An insight into the corrosion mechanism was obtained by examining some of the corroded specimens using SEM and EDS.

Chemical	Concentration (g/L)
Nickel sulphate	20-30
Sodium hypophosphite	14-20
Sodium citrate	35
Ammonium sulphate	30
Lactic acid	5
Sodium tungstate	15-25
Deposition Conditions	
pH	7-8
Bath volume	200 mL
Deposition temperature	90 ± 2 °C
Deposition duration	3 hours
Heat treatment	-
Agitation	-

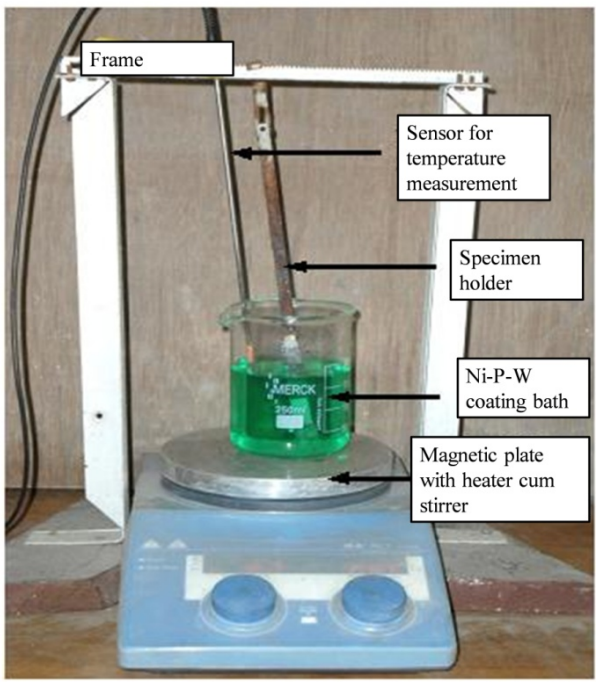

Figure 2. Coating bath along with composition and deposition conditions

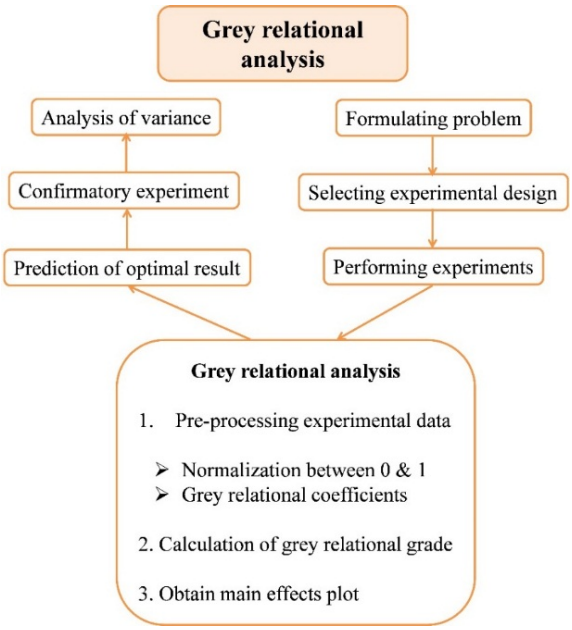

Figure 3. Schematics steps of Grey relational analysis

3. RESULTS AND DISCUSSIONS

3.1 Corrosion performance and its optimization

The corrosion performance of the electroless Ni-P-W coated rebars has been optimized using GRA. The results of corrosion tests following the sequence of L9 OA is shown in Table 3. After the experimental data is obtained, grey relational generation is carried out. Initially, the values of E_{corr} and $I_{corr}$are normalized between 0 and 1. The values are initially normalized because of the in-homogeneity in the range of data values of the multiple responses as well as their units. A nobler value of E_{corr} and lower value of I_{corr} is desirable. Hence, E_{corr} is normalized following higher-the-better quality characteristics (since negative values of corrosion potential are obtained) while I_{corr} is normalized following lower-the-better quality characteristics. Higher the better-quality characteristics are given as:

$$x_i^*(k) = \frac{x_i(k) - \min x_i(k)}{\max x_i(k) - \min x_i(k)} \quad (1)$$

Lower-the-better characteristics are given as:

$$x_i^*(k) = \frac{\max x_i(k) - x_i(k)}{\max x_i(k) - \min x_i(k)} \quad (2)$$

Here min $x_i(k)$ and max $x_i(k)$ are the smallest and largest values of $x_i(k)$ for the k^{th} response, respectively.

Next, the grey relational coefficient (GRC) is found out and is represented by $\xi_i(k)$. The values of GRC for $E_{corr}(\xi_1)$ and $I_{corr}(\xi_2)$ are listed for all the 9 experimental runs in Table 3. The GRC gives a correlation between the experimental data and the ideal best, i.e., 1. Thus, it resembles how far the experimental result is deviating from the ideal value. A GRC value close to 1 resembles near ideal or optimal condition. The GRC $\xi_i(k)$is calculated as follows:

$$\xi_i(k) = \frac{\Delta_{\min} + r\Delta_{\max}}{\Delta_{0i}(k) + r\Delta_{\max}} \quad (3)$$

Here $\Delta_{0i} = ||x_{0i}(k) - x_i^*(k)||$, $\Delta_{min}$is the minimum value of absolute difference while $\Delta_{max}$is the maximum value of the same. The distinguishing coefficient is given by r and is taken to be 0.5 since it is commonly used in GRA because of its moderate distinguishing effects [52].

The multi-performance index is then obtained which is the GRG (represented as γ) and is laid down in Table 3. It is calculated for each row from the average of ξ_1 and ξ_2. The formula is given as:

$$\gamma_i = \frac{1}{n}\sum_{k=1}^{n} \xi_i(k) \quad (4)$$

Here the number of responses is denoted by n and it is 2 in the present case. The order of the GRG is given alongside in Table 3. Highest grade value is order 1 while the lowest is 9. A higher value of GRG suggests that the obtained grade is closer to near optimum parameters [52] and hence has been assigned the order 1. Next, signal to noise (S/N) ratio of the GRG is found out from Taguchi's quality loss function given as follows for higher-the-better criteria:

$$S/N = -10\log\left(\frac{1}{n}\sum\frac{1}{y^2}\right) \quad (5)$$

Here the observed data is represented by y and n is the total number of observations. Since GRG is to be maximized, higher-the-better criterion is employed. The S/N ratio for all the values of GRG is given in Table 3.

Table 3. Results of corrosion tests and grey relational analysis

Sl. No.	E_{corr} (mV)	I_{corr} (μA/cm^2)	Normalized values		Grey relational coefficient		Grade	Order	S/N ratio (dB)
			E_{corr}	I_{corr}	E_{corr}	I_{corr}			
1	-449	5.9	0.0762	0.0000	0.351	0.333	0.342	9	-9.313
2	-255	0.1	1.0000	0.9915	1.000	0.983	0.992	1	-0.073
3	-391	0.5	0.3524	0.9231	0.436	0.867	0.651	5	-3.726
4	-465	0.3	0.0000	0.9573	0.333	0.921	0.627	6	-4.051
5	-271	0.05	0.9238	1.0000	0.868	1.000	0.934	2	-0.594
6	-404	3.28	0.2905	0.4479	0.413	0.475	0.444	8	-7.046
7	-297	1.8	0.8000	0.7009	0.714	0.626	0.670	4	-3.479
8	-362	0.71	0.0000	0.8872	0.333	0.816	0.575	7	-4.812
9	-360	0.07	0.5000	0.9966	0.500	0.993	0.747	3	-2.538

After finding out the *S/N* ratio, the response table for means was obtained and has been laid down in Table 4. This response table (Table 4) contains the mean of *S/N* ratio for every factor at each level. The mean of *S/N* ratio is -3.959 dB. Ranks are assigned in Table 4 based on delta values (subtracting highest and lowest value in a column). Rank 1 has been given to factor C (sodium tungstate concentration) followed by B (sodium hypophosphite concentration) and factor A (nickel sulphate concentration). This indicates that sodium tungstate concentration plays a major role in improving the corrosion performance of the coated steel rebars. Finally, the optimal parametric combination for minimizing corrosion of the coated rebars is predicted from main effects plot given in Fig. 4. The optimal combination is A3B2C2 i.e. 30, 17, 20 g/l of nickel sulphate, sodium hypophosphite and sodium tungstate, respectively.

Statistical analysis of the S/N ratio has been carried out to find out the most influential parameter that affects the corrosion performance of the coated rebars. Analysis of variance (ANOVA) proves to be an efficient tool for the same and the results are laid down in Table 5. Highest contribution is observed for tungstate concentration (factor C) followed by sodium hypophosphite concentration (factor B) at 95 % confidence level. The adequacy of the model at 95% confidence level has been also confirmed from the probability plot of S/N ratio as shown in Fig. 5.

Table 4. Response table of S/N ratios

Level	A	B	C
1	-4.371	-5.614	-7.057
2	-3.897	-1.827	-2.221
3	-3.61	-4.437	-2.6
Delta	0.761	3.788	4.837
Rank	3	2	1
Mean S/N ratio = -3.959 dB			

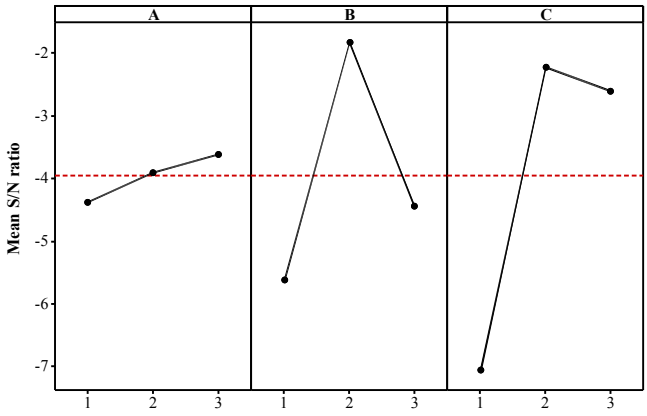

Figure 4. Main effects plot of S/N ratios

Table 5. Analysis of variance of S/N ratios

Source	DOF	Adjusted Sum of Squares	Adjusted Mean Squares	F-Value	Percent Contribution
A	2	0.8861	0.443	1.08	1.310
B	2	22.5446	11.2723	27.44	33.321
C	2	43.4071	21.7036	52.84	64.155
Error	2	0.8216	0.4108		1.214
Total	8	67.6594			100.00
R-sq = 98.79% ; R-sq (adj) = 95.14%					

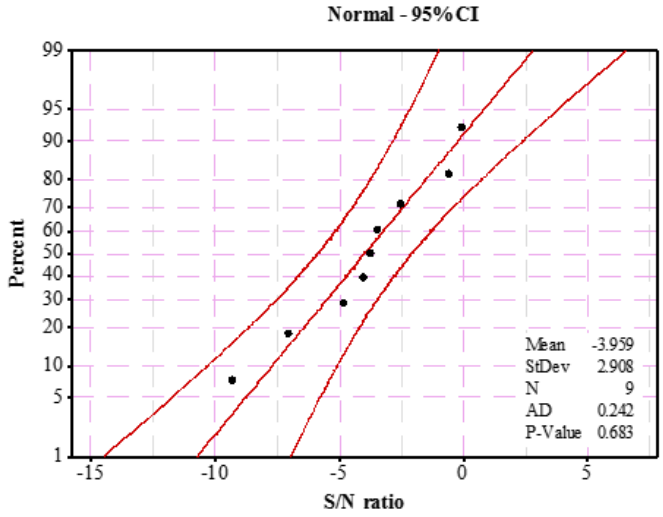

Figure 5. Probability plot of S/N ratios.

Apart from ANOVA, a confirmation test run must be also carried out to establish the adequacy of the optimization problem. For this, the results of E_{corr} and I_{corr} at optimal combination are compared with an initial test run. This initial test run following A1B3C3 combination has been considered based upon previous research work [47] where higher corrosion resistance could be achieved compared to the binary Ni-P or Ni-P-Cu coatings for the said bath composition. The initial test run results are shown in Table 6. Furthermore, a comparison is also made between the experimentally obtained GRG at optimal condition and that predicted by Taguchi analysis. This prediction can be done using the following formula:

$$\hat{\gamma} = \gamma_m + \sum_{i=1}^{i=o} (\bar{\gamma}_i - \gamma_m) \quad (6)$$

Here γ_m is the mean value of GRG, $\bar{\gamma}_i$ is the mean GRG at the optimal levels of process parameters and the number of design variables is represented by o (which is 3 in this case). The confirmatory test results (Table 6) indicate a 51.15 % improvement in grade.

Table 6. Results of the validation test

	Initial	Optimal	
		Predicted	Experimental
Level	$A_1B_3C_3$	$A_3B_2C_2$	$A_3B_2C_2$
E_{corr} (mV)	-391		-258
I_{corr} (μA/cm^2)	0.500		0.065
Grade	0.651	0.961	0.984
Improvement in grade = 0.333 (51.15 %)			

Furthermore, there is a significant improvement in the E_{corr} as well as I_{corr}. The experimentally obtained GRG and Taguchi predicted GRG are also in close agreement. Therefore, a significant improvement may be achieved in the corrosion performance of the electroless Ni-P-W coated steel rebars.

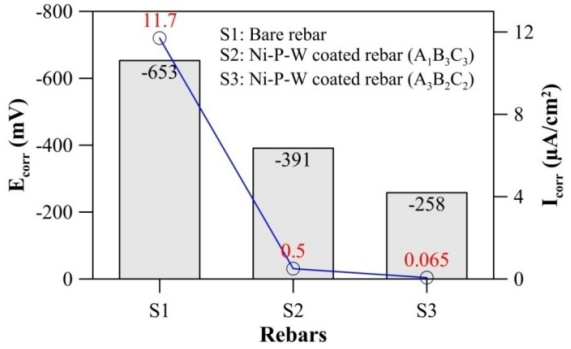

Figure 6. Potentiodynamic polarization parameters of bare and electroless Ni-P-W coated rebar

The PDP parameters of bare rebar, and Ni-P-W coated rebar (mid and optimal condition) in 3.5% NaCl is shown in Fig. 6. The corresponding Tafel plots are shown in Fig. 7. The E_{corr} of steel rebars becomes nobler on application of electroless Ni-P-W coating. There is a significant improvement in E_{corr} at the optimal parametric combination. Furthermore, a noteworthy decrease in Icorr has been also achieved at the optimal coating bath composition compared to the bare steel rebar. The Tafelplots may be also observed for the bare and coated rebars in Fig. 7 which reveals the high corrosion resistance of the coated rebars to pitting attack of chlorides. Thus, active barrier protection to steel rebars may be provided by electroless Ni-P-W coating which is further enhanced on optimizing the bath parameters. Electroless Ni-P based coatings are highly corrosion resistant. This is because the presence of P enhances cathodic and anodic reactions by accelerating dissolution of Ni [47, 48]. Though, passivity could not be observed in the coated rebars in Fig. 7. The potential of the coatings and passivity in chloride induced corrosion in long term may be further investigated in future research works. Nevertheless, the corrosion potential and corrosion current density of the electroless Ni-P-W coated rebars obtained at the optimal bath are comparable to that of conventional epoxy or enamel coated rebars reported in other research works [39-41].

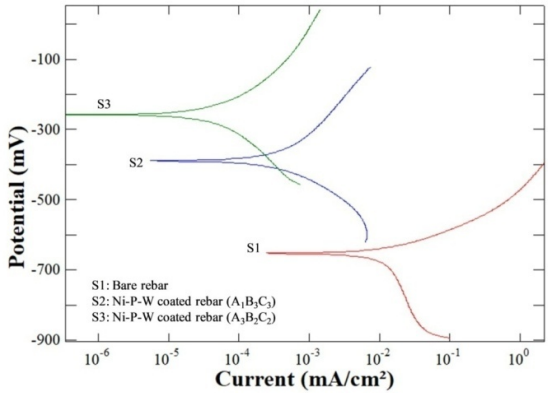

Figure 7. Tafel plots of bare and electroless Ni-P-W coated rebar

3.2 Characterization of Ni-P-W coated steel rebars

The surface morphology of the Ni-P-W coated specimens was studied from SEM images. The results for initial test run (A1B3C3) and optimal combination of parameters (A3B2C2) are shown in Fig. 8 and Fig. 9 respectively. The EDS analysis is also given alongside the SEM images. The surface morphology of electroless nickel coatings is largely dependent on the coating bath parameters. Spherical nodules with large nodulated structures are visible in Fig. 8. From the EDS analysis, the coatings are concluded to be in the higher P range in Fig. 8. At the optimal combination of bath parameters, the W content increases but P content remains almost unchanged. The coatings appear smoother compared to the initial test run and are more compact in Fig. 9. Thus, even though the P content is almost same in both the coatings, there is a difference in W content which leads to microscopically heterogeneous coatings [50, 51]. The cauliflower like appearance can be noticed in Ni-P-W coatings obtained at the initial test run (Fig. 8) along with clear cellular boundaries whereas the coatings are comparatively compact at the optimal condition (Fig. 9). With an increase in W content, the compactness of nodular structure was favored [50]. Also, there is a correlation between coating morphology and corrosion resistance. Coarse structures with specific grain boundaries enhance corrosion and are sites of localized corrosion. Thus, enhanced corrosion resistance of the coated steel rebars at the optimal bath constituents has been reflected in the PDP results (Fig. 7).

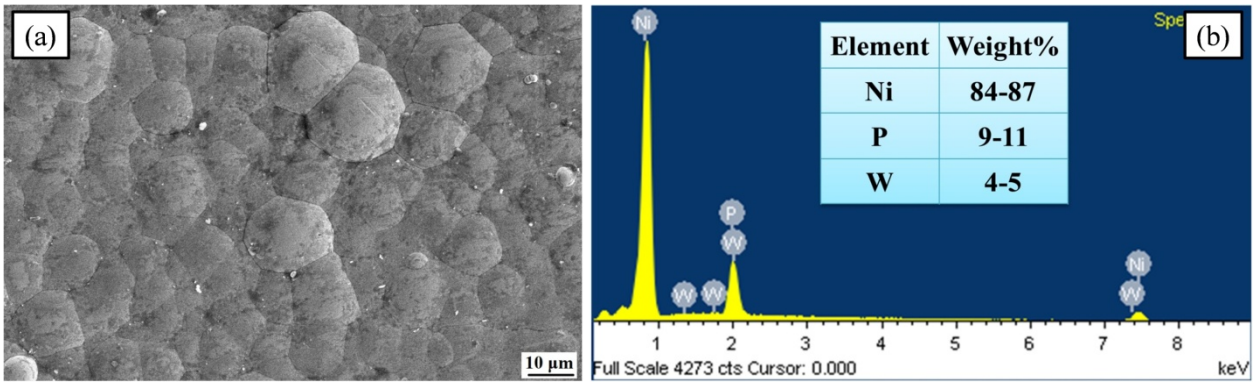

Figure 8. (a) SEM and (b) EDS analysis of Ni-P-W coating at its initial combination of parameters ($A_1B_3C_3$)

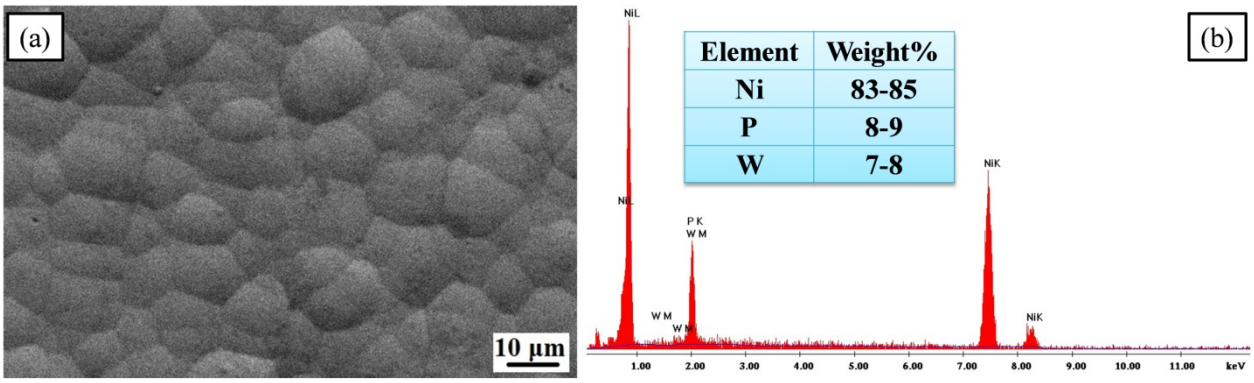

Figure 9. (a) SEM and (b) EDS analysis of Ni-P-W coating at its optimal combination of parameters ($A_3B_2C_2$)

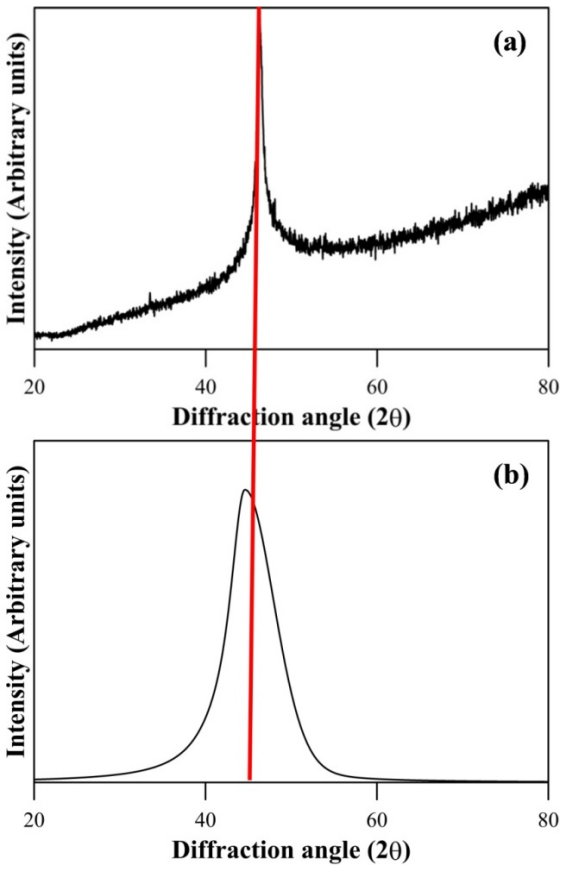

Figure 10. XRD analysis of Ni-P-W coating for the (a) initial test run and (b) optimal parametric combination

The XRD peaks of Ni-P-W coated rebars are shown in Fig. 10. For both the coating bath formulation, a mixture of amorphous/nanocrystalline structure is concluded. A sharp peak superimposed with short ones is centered on 44° 2θ diffraction angle. This sharp reflection has been ascribed to Ni (111) plane [51]. There is marginal variation in the intensity of Ni (111) peak and the full width at half maximum in both the coating variants i.e. initial test combination and optimal combination. This is because of the fact that the structure of Ni-P-W coating is mainly affected by the P content rather than W due to the high solid solubility of W in Ni (40 wt. %) [51]. Thus, due to a relatively same amount of P content, both the coatings exhibit a mixed amorphous/nanocrystalline structure. Although, the surface morphology is affected by W content in the coatings and can be concluded from Figs. 8 and 9.

3.3 Characterization of bare and Ni-P-W coated rebars post corrosion in 3.5% NaCl

The corroded surface of bare rebar is shown in Fig. 11. The surface is characterized by severe pitting in Fig. 11(a). Chloride induced cracks can be also seen in the higher magnification SEM micrograph in Fig. 11(b). Deep pits are observed for the steel rebars when subjected to accelerated corrosion test in chloride environment which indicates poor corrosion resistance. Thus, bare rebars are prone to attack by chloride ions in marine environment which is clearly concluded from Fig. 11.

Electroless Ni-P-W coated rebars obtained from the optimal coating bath composition and subjected to chloride attack is shown in Fig. 13(a) along with its EDS analysis (Fig. 13(b)). The surface is characterized by corrosion products in the form of lamellar structures even though the coating remains undeformed. This corrosion product is expected to be a Ni and W rich oxide layer which provides the protection from severe chloride ion attack. Thus, this is an indication of the

onset of a passive layer which may further develop if the coated rebars are subjected to chloride environment for a higher duration.

The long-term corrosion performance of the Ni-P-W coated rebar in chloride environment may be investigated in future research works. Nevertheless, the formulation of an optimal coating bath composition using GRA has resulted in enhanced corrosion performance compared to bare steel rebars. Hence, Ni-P-W coatings may be considered as an effective and potential candidate for enhancing corrosion performance of rebars used in structures near coastal areas and marine environment. Other nickel based coatings [53, 54] may be considered in future studies to evaluate their efficacy under similar conditions.

4. CONCLUSION

The present work investigated the potential of Ni-P-W coating deposited by electroless method for corrosion prevention of steel rebars in simulated marine environment and accelerated chloride attacks. Fe-600 grade steel rebars were coated with electroless Ni-P-W coating. The coating bath parameters namely the concentration of nickel sulphate, sodium hypophosphite and sodium tungstate were varied. As per the combinations provided in Taguchi's L9 OA, the coatings were deposited. Their corrosion resistance was measured in a three-electrode cell in the presence of 3.5% NaCl. GRA was utilized to predict optimal coating bath formulation. The predicted optimal combination is 30 g/l nickel sulphate, 17 g/l sodium hypophosphite and 20 g/l sodium tungstate. A noble E_{corr} of -258 mV and low I_{corr} of 0.065 μA/cm^2 could be achieved consequently. On the other hand, the bare rebar had -653 mV and 11.7 μA/cm^2 of E_{corr} and I_{corr} respectively. SEM micrograph of Ni-P-W coatings prior to corrosion tests revealed a cauliflower like surface morphology for the initial parametric combination.

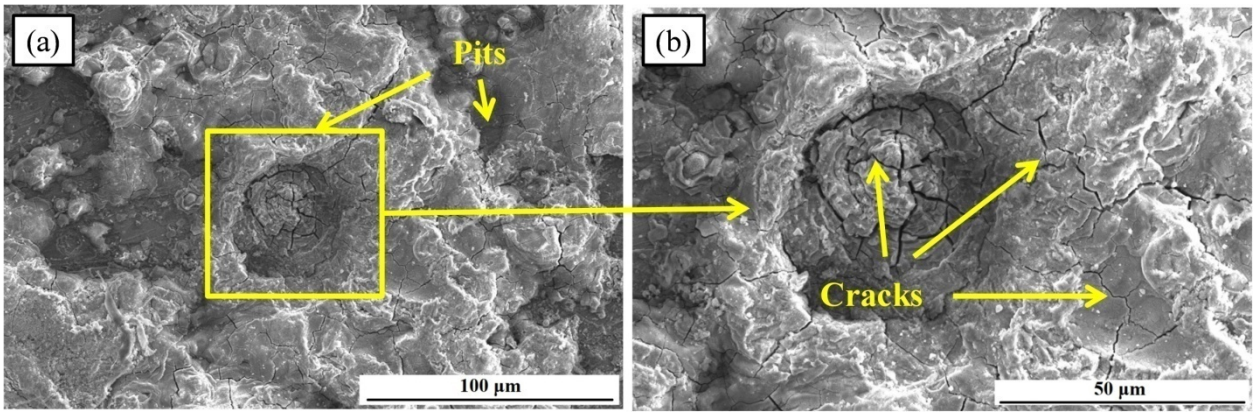

Figure 11. SEM images of (a) corroded bare steel rebar and (b) magnified view of the pit in (a

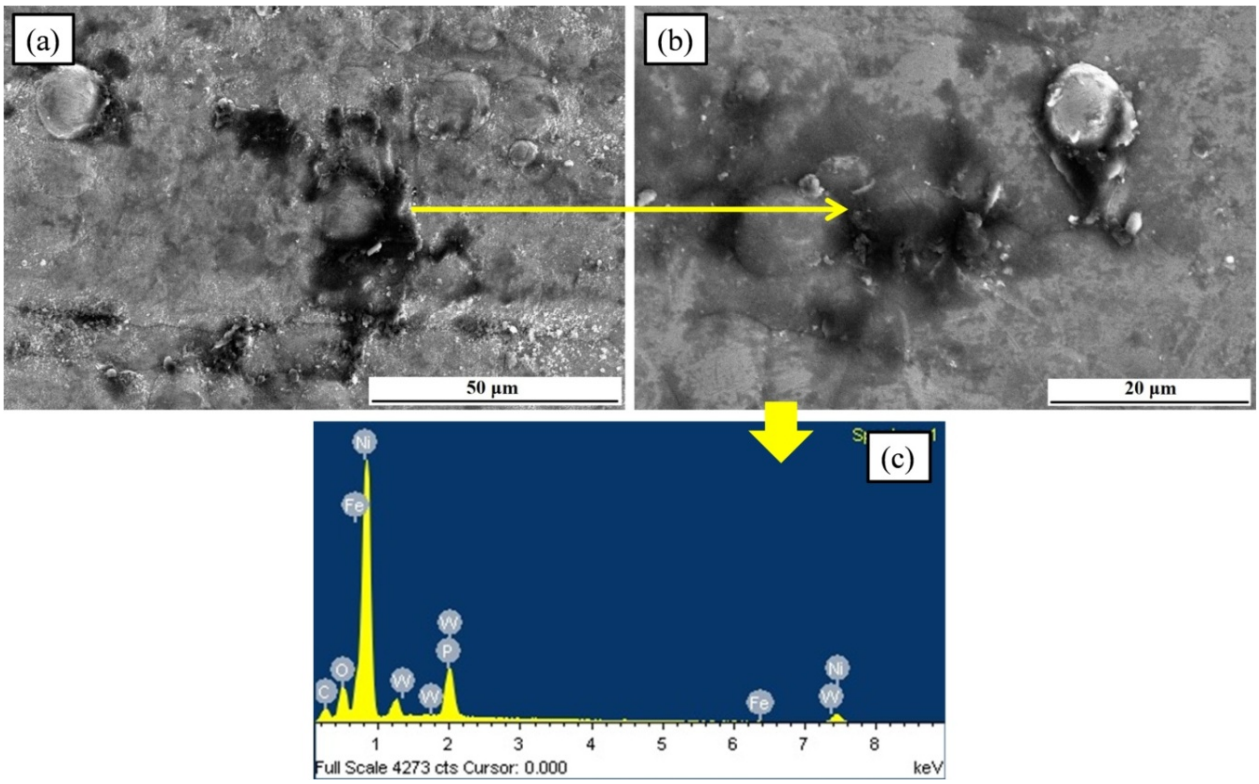

Figure 12. SEM image of (a) corroded Ni-P-W coated rebar for the combination of bath parameters at mid-level and (b) magnified view of the blackish patches in (a). The EDS analysis of blackish patches in (b) is shown in (c)

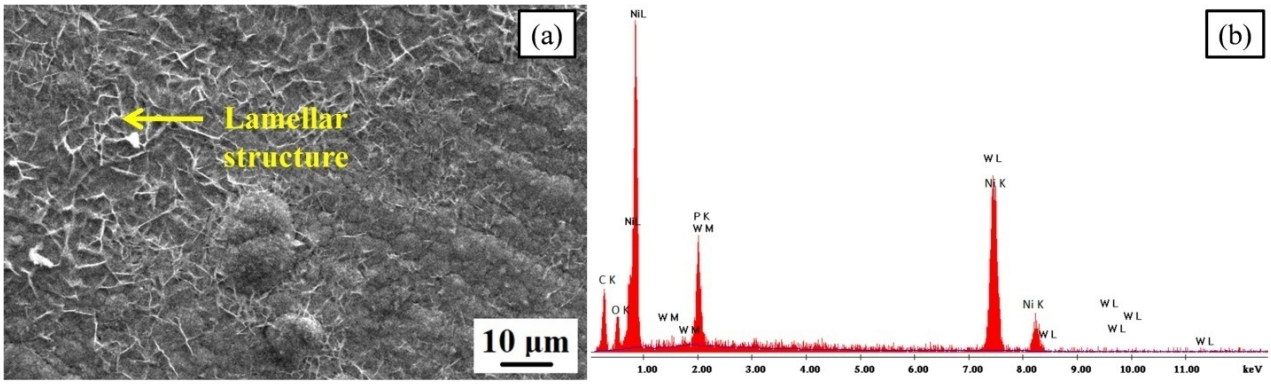

Figure 13. (a) SEM image and (b) EDS of corroded Ni-P-W coated rebar for the bath parameter combination at optimal levels

At the final combination of bath parameters, the coatings were more compact. From the EDS analysis, the coatings were concluded to be in the high-P range. A mixed amorphous/nano-crystalline structure was concluded from XRD analysis. SEM and EDS of Ni-P-W coated rebar (at optimal combination of bath parameters) revealed formation of a protective Ni and W rich oxide film after electrochemical tests. On the other hand, the surface of bare rebar was characterized by severe cracking and pits. Thus, application of Ni-P-W coating from an optimized bath on steel rebars may lead to enhanced lifetime of structuresin marine environment.

ACKNOWLEDGMENT

The authors acknowledge the support of Central Instrumentation Facility (CIF) of Birla Institute of Technology, Mesra, Ranchi 835215, Jharkhand, India, for providing SEM, EDS and XRD facilities.

REFERENCES

[1] Song, Y., Wightman, E., Kulandaivelu, J., Bu, H., Wang, Z., Yuan, Z. and Jiang, G.: Rebar corrosion and its interaction with concrete degradation in reinforced concrete sewers, Water. Res.,Vol. 182, 115961, 2020.

[2] Samson, G., Deby, F., Garciaz, J.L. andLassoued, M.: An alternative method to measure corrosion rate of reinforced concrete structures, Cem. Concr. Compos., Vol. 112, 103672, 2020.

[3] Cabrini, M., Lorenzi, S., Coffetti, D., Coppola, L. andPastore T.: Inhibition effect of tartrate ions on the localized corrosion of steel in pore solution at different chloride concentrations, Buildings, Vol. 10, No. 6, 105, 2020.

[4] Bolzoni, F., Brenna, A., Beretta, S., Ormellese, M., Diamanti, M.V. and Pedeferri M.P.: Progresses in prevention of corrosion in concrete, IOP Conference Series: Earth and Environmental Science,Vol. 296, 012016, 2019.

[5] Sadati, S., Arezoumandi, M. and Shekarchi, M.: Long-term performance of concrete surface coatings in soil exposure of marine environments, Constr. Build. Mater., Vol. 94, pp. 656-663, 2015.

[6] James, A., Bazarchi, E., Chiniforush, A.A., Aghdam, P.P., Hosseini, M.R., Akbarnezhad, A., Martek, I. andGhodoosi, F.: Rebar corrosion detection, protection, and rehabilitation of reinforced concrete structures in coastal environments: A review, Constr. Build. Mater., Vol. 224,pp. 1026-1039, 2019.

[7] Song, Y., Wightman, E., Tian, Y., Jack, K., Li, X., Zhong, H., Bond, P.L., Yuan, Z. and Jiang, G.: Corrosion of reinforcing steel in concrete sewers, Sci. Total. Environ., Vol. 649, pp. 739-748, 2019.

[8] Sagüés, A.A., Pech-Canul, M.A. and Al-Mansur, A.S.: Corrosion macrocell behavior of reinforcing steel in partially submerged concrete columns, Corros. Sci., Vol. 45, pp. 7-32, 2003.

[9] Shi, J., Ming, J.: Influence of defects at the steel-mortar interface on the corrosion behavior of steel, Constr. Build. Mater., Vol. 136, pp. 118-125, 2017.

[10] Pradhan, B. andBhattacharjee, B.: Rebar corrosion in chloride environment, Constr. Build. Mater., Vol. 25, pp. 2565-2575, 2011.

[11] Manera, M, Vennesland, Ø. Bertolini, L.: Chloride threshold for rebar corrosion in concrete with addition of silica fume, Corros. Sci., Vol. 50, pp. 554-560, 2008.

[12] Duarte, R.G., Castela, A.S., Neves, R., Freire, L. and Montemor, M.F.: Corrosion behavior of stainless steel rebars embedded in concrete: an electrochemical impedance spectroscopy study, Electrochim. Acta., Vol. 124, pp. 218-224, 2014.

[13] Sanchez, J., Fullea, J. and Andrade, C.: Corrosion-induced brittle failure in reinforcing steel,Theor. Appl. Fract. Mech., Vol. 92, pp. 229-232, 2017.

[14] Martin, U., Ress, J., Bosch, J. andBastidas, D.M.: Stress corrosion cracking mechanism of AISI 316LN stainless steel rebars in chloride contaminated concrete pore solution using the slow strain rate technique, Electrochim. Acta,Vol. 335, 135565, 2020.

[15] Liu, J., Yu, C., Shu, X., Ran, Q. and Yang, Y.: Recent advance of chemical admixtures in concrete, Cem. Concr. Res., Vol. 124, 105834, 2019.

[16] Ormellese, M., Berra, M., Bolzoni, F.A. andPastore, T.: Corrosion inhibitors for chlorides induced corrosion in reinforced concrete structures, Cem. Concr. Res., Vol. 36, pp. 536-547, 2006.

[17] Duan, P., Shui, Z., Chen, W. Shen, C.: Efficiency of mineral admixtures in concrete: Microstructure, compressive strength and stability of hydrate phases, Appl. Clay. Sci., Vol. 83, pp. 115-121, 2013.

[18] Söylev, T.A., Richardson, M.G.: Corrosion inhibitors for steel in concrete: State-of-the-art report, Constr. Build. Mater., Vol. 22, pp. 609-622, 2008.

[19] De Schutter, G., Luo, L.: Effect of corrosion inhibiting admixtures on concrete properties, Constr. Build. Mater., Vol. 18, pp. 483-489, 2004.

[20] Li, X., Bond, P.L., O'Moore, L., Wilkie, S., Hanzic, L., Johnson, I., Mueller, K., Yuan, Z. and Jiang, G.: Increased resistance of nitrite-admixed concrete to microbially induced corrosion in real sewers, Environ. Sci. Technol., Vol. 54, pp. 2323-2333, 2020.

[21] Baltazar-Zamora, M.A., Bastidas, D., Santiago-Hurtado, G., Mendoza-Rangel, J.M., Gaona-Tiburcio, C., Bastidas, J.M. andAlmeraya-Calderón, F.: Effect of Silica Fume and Fly Ash Admixtures on the Corrosion Behavior of AISI 304 Embedded in Concrete Exposed in 3.5% NaCl Solution, Materials, Vol. 12, 4007, 2019.

[22] Wang, F., Lei, S., Ou, J. and Li, W.: Effect of PDMS on the waterproofing performance and corrosion resistance of cement mortar, Appl. Surf. Sci., Vol. 507, 145016, 2020.

[23] Pan, C., Chen, N., He, J., Liu, S., Chen, K., Wang, P. andXu, P.: Effects of corrosion inhibitor and functional components on the electrochemical and mechanical properties of concrete subject to chloride environment, Constr. Build. Mater., Vol. 260, 119724, 2020.

[24] Lei, L., Li, R. and Fuddin, A.: Influence of maltodextrin retarder on the hydration kinetics and mechanical properties of Portland cement,Cem. Concr. Compos., Vol 114, 103774, 2020.

[25] Ahmad, A., Kumar, R. and Kumar, A.: Effect of sodium molybdate and sodium tungstate in concrete rebar corrosion, Anti-Corros. Methods. Mater., Vol. 66, pp. 253-263, 2019.

[26] Sohail, M.G., Kahraman, R., Alnuaimi, N.A., Gencturk, B., Alnahhal, W., Dawood, M. andBelarbi, A.: Electrochemical behavior of mild and corrosion resistant concrete reinforcing steels, Constr. Build. Mater., Vol. 232, 117205, 2020.

[27] Luo, H., Su, H., Dong, C. and Li, X.: Passivation and electrochemical behavior of 316L stainless steel in chlorinated simulated concrete pore solution, Appl. Surf. Sci., Vol. 400, pp. 38-48, 2017.

[28] Criado, M., Bastidas, D.M., Fajardo, S., Fernández-Jiménez, A. andBastidas, J.M.: Corrosion behaviour of a new low-nickel stainless steel embedded in activated fly ash mortars,Cem.Concr. Compos., Vol. 33, pp. 644-652, 2011.

[29] Liu, M., Cheng, X., Li, X., Pan, Y. and Li, J.: Effect of Cr on the passive film formation mechanism of steel rebar in saturated calcium hydroxide solution, Appl. Surf. Sci., Vol. 389, pp. 1182-1191, 2016.

[30] Tian, Y., Liu, M., Cheng, X., Dong, C., Wang, G. and Li, X.: Cr-modified low alloy steel reinforcement embedded in mortar for two years: Corrosion result of marine field test, Cem.Concr. Compos., Vol. 97, 190-201, 2019.

[31] Pour-Ali, S., Dehghanian, C. andKosari, A.: Corrosion protection of the reinforcing steels in chloride-laden concrete environment through epoxy/polyaniline–camphorsulfonate nanocomposite coating, Corros. Sci., Vol. 90, pp. 239-247, 2015.

[32] Sohail, M.G., Salih, M., Al Nuaimi, N. andKahraman, R.: Corrosion performance of mild steel and epoxy coated rebar in concrete under simulated harsh environment, Int. J. Building Pathology and Adaptation, Vol. 37, pp. 657-678, 2019.

[33] Weishaar, A., Carpenter, M., Loucks, R., Sakulich, A. and Peterson, A.M.: Evaluation of self-healing epoxy coatings for steel reinforcement, Constr. Build. Mater., Vol. 191, pp. 125-135, 2018.

[34] Rajitha, K., Mohana, K.N., Mohanan, A. andMadhusudhana, A.M.: Evaluation of anti-corrosion performance of modified gelatin-graphene oxide nanocomposite dispersed in epoxy coating on mild steel in saline media, Colloids. Surf. A, Vol. 587, 124341, 2020.

[35] Khodair, Z.T., Khadom, A.A. andJasim, H.A.: Corrosion protection of mild steel in different aqueous media via epoxy/nanomaterial coating: preparation, characterization and mathematical views, J. Mater. Res. Technol., Vol. 8, pp. 424-435, 2019.

[36] Zhang, Y.: Electrochemical study on corrosion resistance of epoxy-coated reinforcing steel in bridge concrete, Int. J.Electrochem. Sci., Vol. 14, pp. 9347-9354, 2019.

[37] Tang, F., Chen, G., Brow, R.K., Volz, J.S. andKoenigstein, M.L.: Corrosion resistance and mechanism of steel rebar coated with three types of enamel, Corros. Sci., Vol. 59, pp. 157-168, 2012.

[38] Tang, F., Chen, G., Volz, J.S., Brow, R.K. andKoenigstein, M.L.: Microstructure and corrosion resistance of enamel coatings applied to smooth reinforcing steel, Constr. Build. Mater., Vol. 35, pp. 376-384, 2012.

[39] Tang, F., Cheng, X., Chen, G., Brow, R.K., Volz, J.S. andKoenigstein, M.L.: Electrochemical behavior of enamel-coated carbon steel in simulated concrete pore water solution with various chloride concentrations, Electrochim. Acta, Vol.92, pp. 36-46, 2013.

[40] Tang, F., Chen, G. and Brow, R.K.: Chloride-induced corrosion mechanism and rate of enamel- and epoxy-coated deformed steel bars embedded in mortar,Cem.Concr. Res., Vol.82, pp. 58-73, 2016.

[41] Tang, F., Bao, Y., Chen, Y., Tang, Y. and Chen, G.: Impact and corrosion resistances of duplex epoxy/enamel coated plates, Constr. Build. Mater., Vol. 112, pp. 7-18, 2016.

[42] Wang, Y.Q., Kong, G., Che, C.S. and Zhang, B.: Inhibitive effect of sodium molybdate on the corrosion behavior of galvanized steel in simulated

concrete pore solution, Constr. Build. Mater., Vol. 162, pp. 383-392, 2018.

[43] Fan, L., Meng, W., Teng, L. andKhayat, K.H.: Effect of steel fibers with galvanized coatings on corrosion of steel bars embedded in UHPC, Composites Part. B, Vol. 177, 107445, 2019.

[44] Jaśniok, M., Sozańska, M., Kołodziej, J. andChmiela, B.: A two-year evaluation of corrosion-induced damage to hot galvanized reinforcing steel B500SP in chloride contaminated concrete, Materials, Vol. 13, 3315, 2020.

[45] Pernicova, R., Dobias, D. andPokorny, P.: Problems connected with use of hot-dip galvanized reinforcement in concrete elements, Procedia. Eng., Vol. 2017; pp. 859-866, 2017.

[46] Singh, D.D.N. and Ghosh, R.: Electroless nickel–phosphorus coatings to protect steel reinforcement bars from chloride induced corrosion, Surf. Coat. Technol., Vol. 201, pp. 90-101, 2016.

[47] Mukhopadhyay, A. and Sahoo, S.: Corrosion protection of reinforcement steel rebars by the application of electroless nickel coatings, Engineering Research. Express, Vol. 1, 015021, 2019.

[48] Farzaneh, A., Ehteshamzadeh, M. andMohammadi, M.: Corrosion performance of the electroless Ni–P coatings prepared in different conditions and optimized by the Taguchi method, J. Appl. Electrochem.,Vol. 41, pp.19-27, 2011.

[49] Bureau of Indian Standards. https://bis.gov.in/qazwsx/sti/STI1786PP6.pdf (accessed 5th December 2020).

[50] Oliveira, M.C., Correa, O.V., Ett, B., Sayeg, I.J., Lima, N.B. andAntunes, R.A.: Influence of the tungsten content on surface properties of electroless Ni-W-P coatings, Materials Research, Vol. 21, e20170567, 2018.

[51] Balaraju, J.N. andRajam, K.S.: Surface morphology and structure of electroless ternary NiWP deposits with various W and P contents, J. Alloys. Compd., Vol. 486, pp. 468-473, 2009.

[52] Rajput, V., Pundir, S.S., Goud, M. andSuri, N.M.: Multi-response optimization of ECDM parameters for silica (quartz) using grey relational analysis, Silicon, 2020, doi.org/10.1007/s12633-020-00538-7.

[53] Vite-Torres, J., Vite-Torres, M., Aguilar-Osorio, R. andReyes-Astivia, J.E.: Tribological and corrosion properties of nickel coatings on carbon steel, FME Trans.,Vol. 43, pp. 206-210, 2015.

[54] Sahoo, P. and Das, S.K.: Tribology of electroless nickel coatings – A review, Materials & Design, Vol. 32(4), pp. 1760-1775, 2011.

ИСПИТИВАЊЕ ОСОБИНА КОРОЗИЈЕ КОД ЧЕЛИЧНЕ АРМАТУРЕ ПРИМЕНОМ БЕЗЕЛЕКТРОНСКЕ Ni-P-W ПРЕВЛАКЕ – ОПТИМИЗАЦИОНИ ПРИСТУП КОРИШЋЕЊЕМ ГРЕЈ РЕЛАЦИОНЕ АНАЛИЗЕ

А. Мукхопадхјај, С. Сахо

Истраживане су безелектронске Ni-P-W превлаке као потенцијални материјал за спречавање корозије код челичне арматуре изложене хлоридном окружењу. Потенциодинамичка поларизација је коришћена за испитивање отпорности на корозију код арматура са и без превлаке. Помоћу грејрелационе анализе базиране на Тагучи методу извршено је предвиђање садржаја купатила за таложење превлаке, што би резултирало побољшаном отпорношћу на корозију код арматуре са превлаком. Већи потенцијал корозије и мања густина корозионе струје могла би да се постигне у поређењу са арматуром без превлаке са концентрацијом никла од 30 г/л, натријумхипофосфита од 17 г/л и натријумволфраматом од 20 г/л у купатилу за таложење превлака. Морфологија арматуре са и без превлаке после појаве корозије показала је прскотине на арматури без превлаке. Арматура са Ni-P-W превлаком при оптималном садржају купатила предвиђеном Тагучи методом показала је занемарљиво оштећење у хлоридном окружењу са почецима стварања оксидног слоја.